recycling

MDPI

Article

Study of the Flowability Properties, Morphology and Microstructure of Hazelnut (*Corylus avellana* L.) Shell Waste Particles Obtained by Milling

Israel Arzate-Vázquez [1], Juan Vicente Méndez-Méndez [1,*], Ruth Nohemí Domínguez-Fernández [2], Mayra Beatriz Gómez-Patiño [1], Daniel Arrieta-Baez [1], José Jorge Chanona-Pérez [3], Nayeli Vélez-Rivera [4] and Germán Anibal Rodríguez-Castro [5]

1 Centro de Nanociencias y Micro y Nanotecnologías, Instituto Politécnico Nacional, Luis Enrique Erro s/n, Zacatenco, Ciudad de México 07738, Mexico; iarzate@ipn.mx (I.A.-V.); mbgomez@ipn.mx (M.B.G.-P.); darrieta@ipn.mx (D.A.-B.)
2 Centro Interdisciplinario de Ciencias de la Salud, Unidad Milpa Alta, Instituto Politécnico Nacional, Carretera Xochimilco-Oaxtepec km 39.5, Milpa Alta, Ciudad de México 12000, Mexico; rdominguezf@ipn.mx
3 Departamento de Ingeniería Bioquímica, Escuela Nacional de Ciencias Biológicas, Instituto Politécnico Nacional, Unidad Profesional Adolfo López Mateos, Av. Wilfrido Massieu s/n y cerrada Miguel Stampa, Industrial Vallejo, Ciudad de México 07700, Mexico; jchanona@ipn.com
4 Área Académica de Gastronomía, Instituto de Ciencias Económico-Administrativas, Universidad Autónoma del Estado de Hidalgo, Circuito de la Concepción km 2.5, San Juan Tilcuautla, San Agustín Tlaxiaca, Hidalgo 42160, Mexico; nayeli_velez@uaeh.edu.mx
5 Instituto Politécnico Nacional, SEPI ESIME Zacatenco, Grupo Ingeniería de Superficies, U. P. Adolfo López Mateos, Zacatenco, Ciudad de México 07738, Mexico; garodriguezc@ipn.mx
* Correspondence: jmendezm@ipn.mx; Tel.: +52-55-57296000 (ext. 57506)

Abstract

Mechanical milling is a relevant preliminary processing operation that is widely used for the reuse of various types of agro-industrial waste. The objective of this study was to conduct milling experiments of hazelnut (*Corylus avellana* L.) shell waste at different times (0.5, 1 and 1.5 min) and subsequently evaluate the particle size distribution (PSD) of the powders obtained by sieving methodology. In addition, flowability parameters were determined for the particles retained on the sieves, and their morphology and microstructure were examined using several microscopy techniques. The results demonstrated that the hazelnut shells were successfully fractionated under the milling conditions investigated (short milling times $\leq$ 1.5 min), and the histograms of the PSD exhibited a wide dispersion of sizes ($\leq$1.7 mm). The particles retained from sieve$_{100}$ to residue exhibited poor or no flow, attributable to the high degree of cohesion between them. Morphological analysis based on optical microscopy and image analysis revealed that there was an increase in the aspect ratio parameter when the particle size decreased, meaning that the particles had elongated shapes. Microscopic analysis (SEM, AFM and CLSM) showed that the particles exhibited complex shapes and a comparable microstructure, comprising tightly packed clusters of sclerenchyma cells. From the microscopy images obtained (SEM and AFM), it was inferred that the cracks generated during blade impacts propagate along the middle lamella of the cells, allowing the cluster-like arrangement to be preserved. The CLSM results demonstrated that as the size of hazelnut shell particles decreases, the exposure of lignin on its surface is favored. The findings of this study demonstrate that hazelnut shell waste can be readily pre-processed using a blade grinder, thereby facilitating its reuse in applications that demand fine particle sizes (e.g., bioadsorption of pollutants and the production of biocomposite materials). Likewise, the results concerning the flowability parameters, microstructural arrangement, and morphological features of the different particle fractions obtained are crucial variables that must be considered. These variables

Academic Editor: Denis Rodrigue

Received: 28 November 2025
Revised: 12 December 2025
Accepted: 19 December 2025
Published: 22 December 2025

significantly influence the possible applications for the revalorization of this type of agro-industrial waste.

Keywords: agro-industrial waste; hazelnut shells; flowability; microstructural features; microscopy techniques

1. Introduction

In recent decades, there has been a substantial increase in the volume of agro-industrial waste, which is mainly attributed to the global growth in food demand. Agro-industrial waste is defined as all materials discharged by the agricultural and food industries, produced through activities related to harvesting, cleaning, handling, and processing food. Examples of these types of waste include, but are not limited to, leaves, roots, fruit peels, nutshells, seeds, eggshells, bagasse, rice husk and stems [1]. The absence of comprehensive health strategies and regulations in several countries, including Mexico, has led to the utilization of unsuitable waste disposal methods, such as burning or landfill, which has significantly contributed to the exacerbation of environmental concerns. Until a few years ago, agro-industrial waste was considered worthless material, so its use was quite limited. In terms of chemical composition, this type of biological material has high concentrations of proteins, carbohydrates, biopolymers, minerals, and functional compounds [2]. However, these materials have the potential to play a fundamental role as renewable resources, which contributes to reducing waste accumulation and preventing environmental pollution, in accordance with the principles of the circular economy [3]. Currently, the implementation of production systems, such as the circular economy, has emerged as a priority. These strategies promote the utilization, reuse, and recycling of this type of waste. One type of agro-industrial waste that has generated considerable interest in recent years is hazelnut shells. These materials are notable for their abundance, chemical composition, and favorable mechanical properties.

Hazelnuts (*Corylus avellana* L.) are one of the most important nuts worldwide produced and the second most popular after almonds. Hazelnuts are grown in many countries in Europe and Asia, with Turkey, Italy, United States, and Azerbaijan standing out for their production and exportation volume [4]. The hazelnut shell is a thin brown structure that protects the edible seed, known as the kernel. This structure represents approximately 50% of the total fruit weight [5]. Given the estimated annual production of hazelnuts at 1,195,732 tons, the amount of shell waste generated is estimated to be approximately 538,559 tons [3]. In regard to the chemical composition of shells, McNeill et al. [3] conducted a summary of the chemical composition of various types of nut shells, noting that hazelnut shells have the following composition: lignin (30–38%), cellulose (17–24%), hemicellulose (15–28%), and moisture content (9%). On the other hand, hazelnut shells are classified as multi-cellular structures, comprising various structural elements such as calcium oxalate crystals, large rounded sclereids, collapsed vascular bundles, and small sclereids [6]. Hazelnut shells have emerged as promising material due to their distinctive characteristics, which have generated significant potential for diverse applications. Hazelnut shells have been utilized in a variety of applications, including the synthesis of biosorbents for the removal of pollutants [7], the production of activated carbon [8,9], as base material for the synthesis of cellulose nanostructures [10], as fillers for the production of biocomposite materials [11], and as biomass for energy production [12]. Additionally, hazelnut shells have been employed in the production of cement compounds [13].

To maximize the potential of agro-industrial waste, several pretreatment methods are employed. Milling is an example of physical pretreatment whose main objective is to reduce particle size through the action of mechanical forces of impact or friction. However, it can also be used to mix and modify the shape of particles [14]. Furthermore, it has been demonstrated that high-energy ball milling can influence the degree of polymerization and crystallinity of cellulose, while altering the rigid structure of agro-industrial waste [15]. To successfully reduce the particle size of agro-industrial waste, various parameters of the milling process must be considered, as well as the intrinsic properties of the waste. The variables to be considered in the milling process include the type of mill, the effective milling time, the amount of the sample in the milling chamber, the milling speed, and the conditions (wet or dry) [16]. Also, the mechanical properties, chemical composition, moisture content, and structural characteristics of the tissues comprising agro-industrial waste must be considered during the milling. The range of particle sizes that is required during the milling process is determined by the specific application for which the waste is to be utilized. For instance, in the elaboration of composite materials based on hazelnut shells, the incorporation of fine particles (mean particle size $\leq$ 110 µm) is advantageous due to their increased surface area [1]. On the contrary, the presence of fine particles (particle size $\leq$ 500 µm) has been shown to be disadvantageous when the hazelnut shells are utilized as biomass for energy production, as fine particles have been observed to cause losses in the performance of burning systems [17]. The manufacture of acoustic panels is another example of an application where the particle size of hazelnut shells directly influences acoustic performance. In this case, moderate milling is sufficient to obtain coarse particles (sizes in the range of mm, $\geq$5 mm), which are easy to handle and have adequate adhesion [18]. Therefore, it is imperative to study the particle size distribution obtained when fragmenting agro-industrial waste under specific milling conditions (e.g., milling time, mill type, etc.). Although milling is a widely used method for the management and utilization of hazelnut shell waste, there is a paucity of literature focusing on comprehensive analysis of this process and the fragmentation mechanisms that occur. Furthermore, there are few studies in the literature that examine in detail the morphological and microstructural characteristics, chemical composition, and physicochemical properties of hazelnut shell particles. Therefore, the objective of this study was to conduct experiments milling hazelnut shells (*Corylus avellana* L.) at different times (0.5, 1, and 1.5 min) and evaluate the particle size distribution (PSD) of the powders obtained using a sieving methodology. Furthermore, the flowability parameters of the particles retained in the sieves utilized were determined, and their morphology and microstructure were examined using several microscopy techniques.

2. Results and Discussion

2.1. Particle Size Distribution (PSD) of Milled Hazelnut Shell Samples

From a technological perspective, it is important to know the particle size distribution of an agro-industrial waste that is subjected to specific milling conditions. In this study, experiments were conducted to mill hazelnut shell waste at various times (0.5, 1, and 1.5 min). The sieving methodology was developed to evaluate the PSD, where for all samples evaluated the recovered material was 99.01 $\pm$ 0.00%. Figure 1 presents the histograms of the PSD of hazelnut shells that were subjected to different milling times. As can be seen in this figure, the histograms exhibit a left-skewed normal distribution, which means that there is a greater dispersion of fine particle sizes. The highest mass retention was observed on the sieve$_{50}$ for the three milling times evaluated, except for the sieve$_{25}$ at 0.5-min milling, which exhibited a mass fraction of approximately 35%. The particles retained on sieve$_{50}$ ranged in size from 300 to 710 µm. The results also revealed that there was a progressive

increase in the mass fraction retained on the higher mesh number sieves ($sieve_{100}$, $sieve_{200}$, $sieve_{400}$) and residue as the milling time increased.

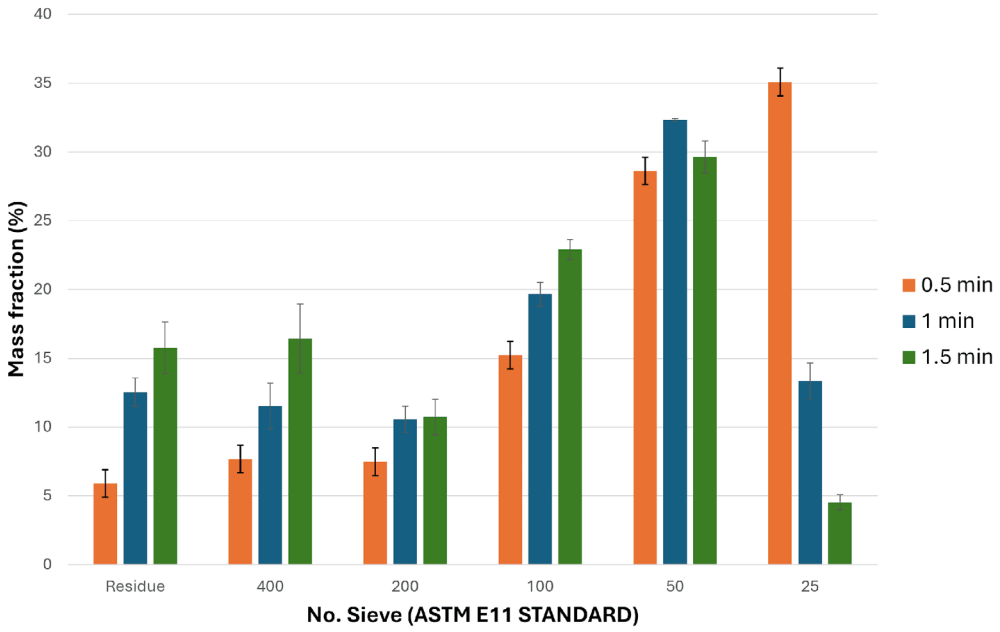

Figure 1. Histograms that represent the particle size distribution (PSD) of hazelnut shell samples that were milled at different times: 0.5, 1 and 1.5 min.

Table 1 presents the granulometry parameters that serve to quantitatively characterize the milled hazelnut shell samples. As expected, a decrease in D_{mean} was observed with increasing milling time, with the following sequence of values: 615.98 µm (0.5 min) > 390.31 µm (1 min) > 281.58 µm (1.5 min). There were significant differences ($p \leq 0.05$) between the D_{mean} values for the different times evaluated. Likewise, high σ values were presented for all milling conditions and these also decreased with increasing time. This fact is associated with the wide dispersion of particle sizes generated by the milling process. Finally, the *span* is a parameter that measures the spread of the distribution, and the values are presented in Table 1. The three distributions exhibited elevated *span* values, ranging from 2.86 to 3.23 for times of 1.5 and 1 min, respectively. These high *span* values are also related to the extensive distribution of particle sizes generated.

Table 1. Parameters determined to characterize the granulometry of milled samples of hazelnut shells at different times.

Milling Time (Minutes)	Parameters of Granulometry		
	Average Particle Size, D_{mean} (µm)	Standard Deviation, σ (µm)	*Span* (Dimensionless)
0.5	615.98 ± 29.72 [a]	768.68 ± 26.17 [a]	2.91 ± 0.09 [b]
1	390.31 ± 14.01 [b]	368.00 ± 10.84 [b]	3.23 ± 0.14 [a]
1.5	281.58 ± 11.20 [c]	316.78 ± 71.27 [b]	2.86 ± 0.07 [b]

The values were expressed as mean ± standard deviation (n = 5). Values with the same letter within the same column indicate no significant differences (Tukey test; $p \geq 0.05$).

The type of mill and milling variables (e.g., time, amount of material, milling speed, wet or dry conditions and temperature) are key factors influencing the particle size distribution (D_{mean}, σ and *span*) of a particulate material [16]. In this regard, a reduction in the particle size of hazelnut shells was successfully achieved by using a blade mill that operated at a constant rotational speed and short milling times. The results indicated that increasing the milling time by a factor of three (i.e., 1.5 min) resulted in a reduction of

approximately 50% in the D_{mean} value (281.58 ± 11.20 µm). Likewise, a similar behavior was observed in the σ values, where it was observed that for the milling time of 1.5 min the σ value decreased to 316.78 ± 71.27 µm. This finding indicates that particle size tends to exhibit greater homogeneity when milling time is increased. These results confirm the significance of time as a pivotal variable in the milling. Despite the plethora of studies published that have focused on the utilization and novel applications of hazelnut shells, only a limited number of studies have reported results on the particle size distribution of this agro-industrial waste. For instance, Barczewski et al. [1] evaluated the application of different types of agro-industrial wastes (sunflower husk, hazelnut shell and walnut shell) as fillers in the development of resin-based composite materials. The authors reported that the milled hazelnut shells sample had a mean particle size value of 47.6 µm and that the PSD exhibited a very narrow shape with particle sizes less than 150 µm. These results are lower than those reported in our study. These differences can be attributed to the milling conditions employed in the aforementioned study, where it is hypothesized that the milling time was considerably longer because this information was not reported in the methodology. In another study, Aliotta et al. [11] produced PLA-based biocomposites using two samples of milled hazelnut shells of different granulometry (coarse and fine). The authors reported that the average diameter values for the coarse and fine particle size samples were 206.7 µm and 25.8 µm, respectively. The coarse particle size value reported by the authors is comparable to that reported in our study for a milling time of 1.5 min (281.58 µm). The authors also noted that both samples exhibited a wide distribution of particle sizes; this behavior is similar to the results found in our study. A notable omission in this study is the lack of information regarding the milling times applied to the two samples of hazelnut shells. Various published studies focused on the reuse of hazelnut shells do not reveal details of the milling conditions used. This fact can be attributed to the utilization of a specific particle size range in these studies, which is obtained through the process of sieving.

2.2. Flowability Parameters of Particulate Samples from Hazelnut Shells

Table 2 presents the values of the physical parameters related to the flowability of the hazelnut shell particles retained in the different sieves. The results indicated that the apparent density (ρ_A) values gradually decreased when the particle size was finer (i.e., larger sieve numbers). The particles retained on sieve$_{25}$ exhibited an ρ_A value of 0.65 ± 0.01 g/cm^3, while the residue particles showed a value of 0.39 ± 0.01 g/cm^3 ($p \leq 0.05$). The decrease in ρ_A values can be attributed to the presence of numerous free spaces, or interparticle spaces, within fine particle powders. This characteristic results in a reduction in the mass occupying a given volume. The tapped density (ρ_T) is a measure of the capacity of the particles of a sample to rearrange and occupy a smaller volume under the action of blows or vibrations. In this sense, it was observed that the ρ_T values were higher compared to the ρ_A values, indicating that there was a rearrangement of the particles. The particles retained from the sieve$_{25}$ to sieve$_{200}$ presented ρ_T values ranging from 0.71 g/cm^3 to 0.74 g/cm^3. No significant differences ($p \geq 0.05$) were observed between these values. The particles retained on the sieve$_{400}$ and in the residue exhibited values of 1.01 ± 0.10 g/cm^3 and 1.89 ± 0.09 g/cm^3, respectively. This finding indicates a higher degree of particle rearrangement in both samples.

Table 2. Physical parameters that describe the flowability of the hazelnut shell particles retained in the sieves used.

Standard Sieve No.	Apparent Density, ρ_A (g/cm^3)	Tapped Density, ρ_T (g/cm^3)	Carr Index, *CI* (%)	Hausner Ratio, *HR*	Angle of Repose, *AOR* (°)	Flow Character of Powders
$Sieve_{25}$	0.65 ± 0.01^{a}	0.72 ± 0.03^{c}	10.33 ± 4.16^{df}	1.11 ± 0.05^{c}	23.86 ± 3.64^{d}	Excellent
$Sieve_{50}$	0.59 ± 0.01^{ab}	0.71 ± 0.01^{c}	17.34 ± 3.21^{ef}	1.21 ± 0.04^{c}	32.31 ± 1.36^{c}	Fair
$Sieve_{100}$	0.51 ± 0.02^{ab}	0.74 ± 0.07^{c}	30.33 ± 9.07^{ce}	1.45 ± 0.19^{c}	33.34 ± 2.05^{c}	Poor
$Sieve_{200}$	0.46 ± 0.01^{ab}	0.71 ± 0.05^{c}	35.00 ± 6.24^{c}	1.54 ± 0.14^{b}	36.17 ± 0.46^{bc}	Very poor
$Sieve_{400}$	0.43 ± 0.02^{ab}	1.01 ± 0.10^{b}	56.66 ± 6.65^{b}	2.34 ± 0.33^{b}	39.74 ± 1.31^{b}	No flow
Residue	0.39 ± 0.01^{b}	1.89 ± 0.09^{a}	79.33 ± 1.52^{a}	4.85 ± 0.36^{a}	48.64 ± 0.43^{a}	No flow

The values were expressed as mean ± standard deviation (n = 5). Values with the same letter within the same column indicate no significant differences (Tukey test; $p \geq 0.05$).

On the other hand, the values of the Carr index (*CI*) and Hausner ratio (*HR*) showed a comparable trend, with an increase in both parameters observed as the particle size decreased. *CI* and *HR* are parameters that are traditionally determined to classify the flow character of powders of different chemical nature [19–21]. Therefore, the particles retained on the $sieve_{25}$ and $sieve_{50}$ showed excellent and fair flow character, respectively. Both samples have a low degree of cohesiveness, allowing particles to flow freely. On the contrary, it was observed that from the $sieve_{100}$, the particles have a poor flow character to no flow ($sieve_{400}$ and residue). The above indicates that these samples have too much cohesiveness between their particles and, as a result, low flowability. Finally, the angle of repose (*AOR*) is another indicator of flowability and as expected it showed a similar trend to the *CI* and *HR* values. The *AOR* values ranged from 23.86° ($sieve_{25}$) to 48.64° (residue). Powders with a high value for the *AOR* indicate a higher degree of cohesion between their particles. From our knowledge, there is little information in the literature on the values of the flowability parameters of hazelnut shell powder or other types of nuts. However, flowability parameter values have been reported for other types of agro-industrial waste. For instance, Jan et al. [2] reported *HR* values of less than 1.12 for potato peel powder, deoiled rice bran, banana peel powder, and paddy husk; these values are very similar to the value reported in our study for the hazelnut shell particle sample from $sieve_{25}$ (see Table 2). The same authors determined *AOR* values for their samples that were similar to or lower than those reported for the hazelnut shell particles of the $sieve_{25}$ (23.86°), except for the paddy husk sample, which had a value of 30.96°.

In general, the flowability of particulate materials or powders depend on various factors such as particle size, particle morphology, temperature and moisture content [22]. Of the factors mentioned above, particle size is one of the physical characteristics that has the greatest influence on the flow character of a powder [23]. Based on the results obtained, it was observed that the smallest hazelnut shell particles had poor to very limited flow characteristics due to the high degree of cohesiveness between the particles. This phenomenon is related to the fact that smaller particles have a greater surface area, which promotes more interparticle interactions (e.g., van der Waals forces and electrostatic forces). From an industrial perspective, it is imperative to understand the flow behavior and cohesion degree of powders because these characteristics influence a range of technological operations, including transport, storage, packaging, blending, and filling.

2.3. Morphological Analysis of Particles by Image Analysis

Table 3 summarizes the values of the particle size and shape parameters of the particles retained on the sieves as calculated by the image analysis technique. As expected, the values of the size parameters (area, perimeter and Feret's diameter) decreased as a function of the mesh opening of the sieves used. These parameters are suitable descriptors of particle size because they also consider the complexity of their shapes. The Feret's diameter is a parameter commonly used to evaluate the equivalent particle diameter. The values of this

parameter show that a wide range of particle sizes from about 1.2 mm ($sieve_{25}$) to 10 µm (residue) was obtained from the milling experiments. On the other hand, some shape parameters were also calculated which showed differences in the retained particles for each of the sieves. Circularity is a descriptor that evaluates the similarity of a particle to a perfect circle; a circularity value of 1 represents a perfect circle, while values closer to 0 indicate elongated shapes. With respect to this parameter, it was observed that the particles retained in most of the sieves had very similar values of circularity (0.64 to 0.70), except for the residue, which had the highest value (0.83), indicating that the particles are more similar to a perfect circle. Aspect ratio was another shape parameter that was determined, which is a measure of the fit of a particle's shape to an ellipse (major axis/minor axis). Therefore, more elongated shapes are seen in the finer particles corresponding to the $sieve_{400}$ and the residue. Finally, we calculated the roundness parameter which is an inverse descriptor of the aspect ratio. As expected, the results for this parameter showed an opposite behavior to the aspect ratio values, with the highest value for particles retained on the $sieve_{25}$ (higher roundness). Particle shape can play an important role in some physical properties of powders, such as flowability. Particles with spherical or rounded shapes can flow better compared to particles with irregular or complex shapes (e.g., polyhedric shapes) [22]. Furthermore, the shape of the particles can be a very important physical characteristic when proposing new uses or applications for this type of agro-industrial waste.

Table 3. Size and shape parameters of hazelnut shell particles retained in different sieves calculated by image analysis.

Standard Sieve No.	Number of Data	Size Parameters			Morphological Parameters (Dimensionless)		
		Area (µm²)	Perimeter (µm)	Feret's Diameter (µm)	Circularity	Aspect Ratio	Roundness
$Sieve_{25}$	50	720,152 ± 103,873	3623 ± 429	1191 ± 181	0.70 ± 0.09	1.29 ± 0.15	0.78 ± 0.09
$Sieve_{50}$	64	154,134 ± 104,302	1631 ± 568	516 ± 177	0.66 ± 0.07	1.36 ± 0.22	0.75 ± 0.11
$Sieve_{100}$	78	50,849 ± 33,631	953 ± 348	311 ± 118	0.67 ± 0.08	1.43 ± 0.38	0.73 ± 0.14
$Sieve_{200}$	201	11,856 ± 5439	456 ± 119	155 ± 40	0.66 ± 0.08	1.49 ± 0.37	0.70 ± 0.14
$Sieve_{400}$	3946	293 ± 93	76.72 ± 19.28	27.57 ± 6.18	0.64 ± 0.17	1.75 ± 0.67	0.62 ± 0.15
Residue	4152	53.28 ± 45.52	26.66 ± 12.64	10.63 ± 4.64	0.83 ± 0.12	1.69 ± 0.53	0.63 ± 0.15

The values were expressed as mean ± standard deviation.

2.4. Microstructural Analysis of the Particles by SEM

The morphology and microstructure of hazelnut shell particles were examined using the SEM technique (Figure 2). In terms of morphology, it has been observed that the particles have a complex and irregular shape. In general, most of the particles are slightly elongated, which is consistent with the values obtained for the aspect ratio parameter, where an increase in this parameter was observed when the particles were finer (see Table 3). Regarding the microstructure, it was observed that particles from the $sieve_{25}$ to $sieve_{200}$ had a similar microstructure consisting of tightly packed clusters of sclerenchyma cells (Figure 2a–d). Morphologic differences in the sclerenchyma cells that make up the particles could be seen in the images. Figure 2c shows particles composed of short isodiametric cells, elongated cells (rod-like shape), and a combination of both. As illustrated in Figure 2d, the particles exhibit a discernible cluster-like architecture, comprising multiple sclerenchyma cells. In the case of the $sieve_{400}$ (Figure 2e), it was observed that the particles correspond to relatively large single cells (65.99 ± 14.78 µm) with isodiametric and elongated shapes; some clusters formed by a few small cells (25.28 ± 5.85 µm) were also seen. Lastly, whole and fractured isodiametric single cells (27.57 ± 5.73 µm) were observed in the residue sample (Figure 2f). In this sample, some elongated cells were also visible. Their width and length were 21.08 ± 4.49 µm and 77.31 ± 12.54 µm, respectively. The high values of circularity and aspect ratio found in the residue (see Table 3) are associated with isodiametric and elongated cells. In addition, many cell wall fragments were observed in the images of the residue (Figure 2f).

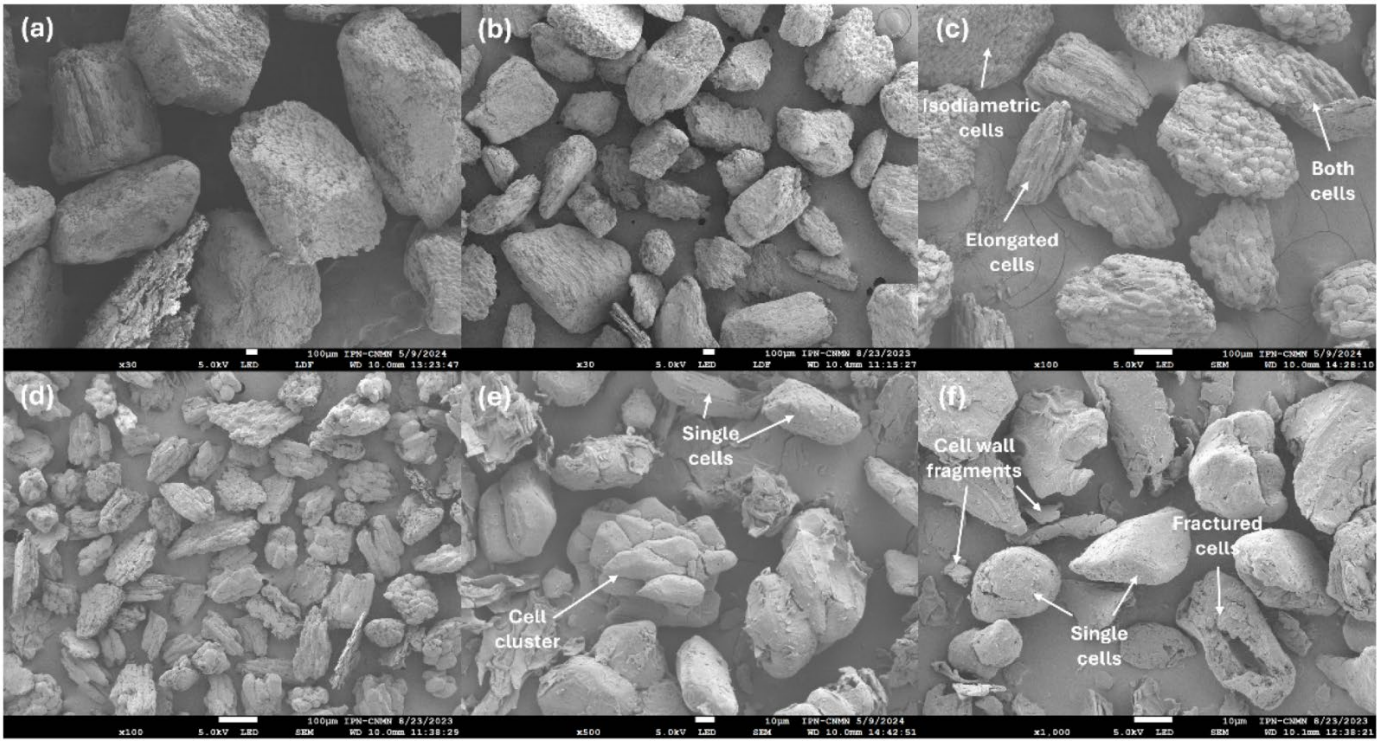

Figure 2. SEM images at different magnifications of hazelnut shell particles retained on each of the sieves used: (**a**) sieve$_{25}$, (**b**) sieve$_{50}$, (**c**) sieve$_{100}$, (**d**) sieve$_{200}$, (**e**) sieve$_{400}$ and (**f**) residue.

Several studies published in the literature indicate that hazelnut shell particles have irregular shapes and rough surfaces [1,11,17]. However, the microstructure of the particles is poorly described in these studies. To accurately describe the microstructural arrangement of particles obtained from agro-industrial waste, it is necessary to know the native structure of the material in detail. Huss et al. [6] classified the hazelnut shell as a multi-cell type structure because it is composed of calcium oxalate crystals, rounded sclereids, vascular bundles and small sclereids. This description agrees with the structural elements observed in the SEM images, with sclereids being the most abundant structures compared to the other structural elements. Sclereid cells constitute the primary structural components of hazelnut shell particles. Some calcium oxalate crystals and fragments of vascular bundles were seen in small proportions in the SEM images of hazelnut shell particles.

On the other hand, SEM images provide information to elucidate the possible fragmentation mechanism occurring in the hazelnut shell during milling process (Figure 3). As mentioned above, the hazelnut shell is a material composed mainly of sclerenchyma cells: short isodiametric cells and elongated cells (rod-like shape). As shown in Figure 3a, these cells are connected by the middle lamella, which is an interfacial matrix that acts as a glue between the cells. This image also shows the presence of pits on the cells, which are randomly distributed and act as a transport system for nutrients and water between cells [24]. The middle lamella serves to maintain the structural integrity of plant tissues and is an approximately 50 nm thick structure [25]. The preservation of the same microstructural arrangement (i.e., tightly packed clusters of sclerenchyma cells) in most of the particles obtained suggests that impact-induced cracks propagate mainly along the middle lamella. Therefore, it can be concluded that middle lamella breakage is the predominant energy-absorbing mechanism responsible for the fragmentation of the hazelnut shell. A characteristic of this mechanism is that the primary cell wall remains nearly intact, as evidenced in Figure 3a. Based on these results, it can be inferred that the cells are weakly linked by the middle lamella, this allows cracks to propagate around the cells. This same

energy- absorbing mechanism has been described by other authors for shells with plant tissues of similar architecture that were subjected to compression and tension tests [6,26].

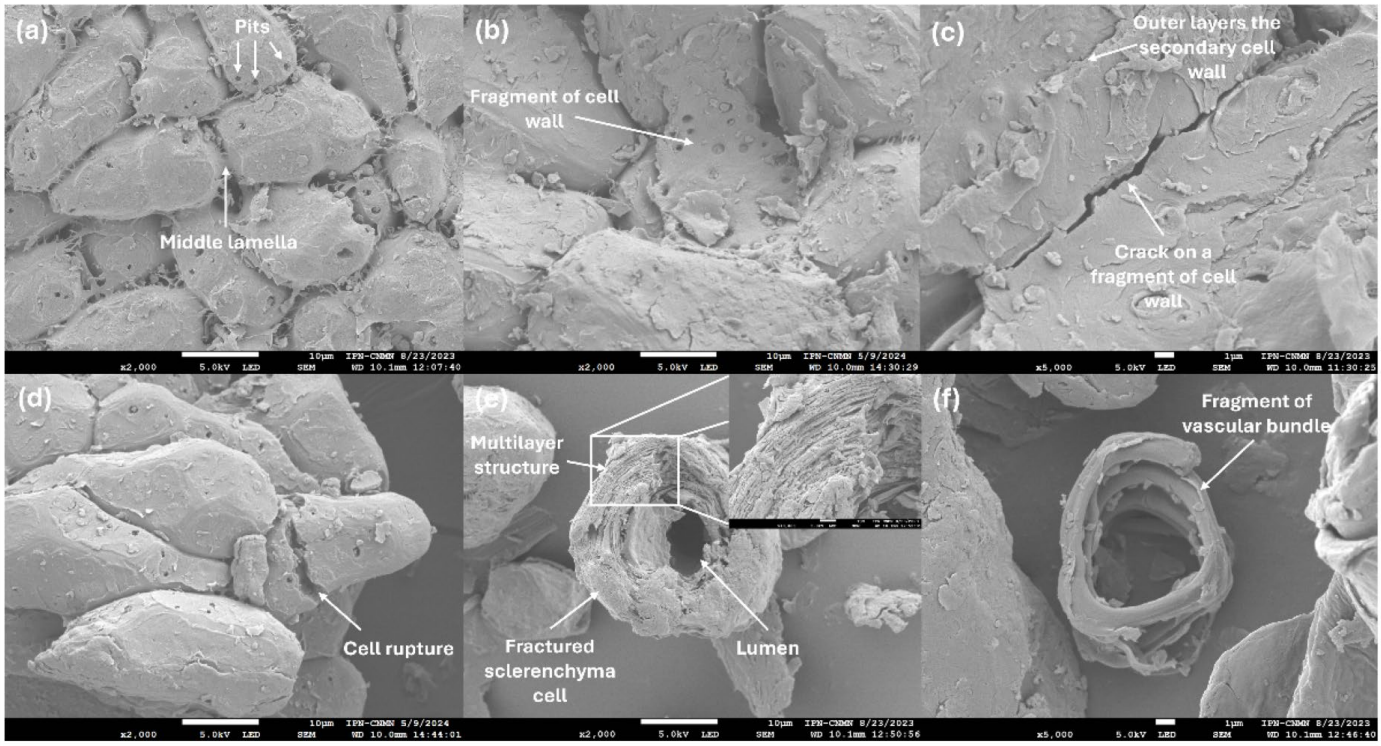

Figure 3. SEM images of microstructural features of hazelnut shell particles and identified failure mechanisms: (**a**) sclerenchyma tissue (sieve$_{200}$), (**b**) fragment of cell wall (sieve$_{100}$), (**c**) micro-crack on cell wall fragment (sieve$_{50}$), (**d**) cell rupture (sieve$_{400}$), (**e**) fractured sclerenchyma cell (residue) and (**f**) fragment of vascular bundle (residue).

The breakage of the primary cell wall is another failure mechanism that was identified in the SEM images. Figure 3b shows a fragment of primary cell wall, which exhibits multiple pits distributed across its surface. The morphology of the fragment suggests that the cell underwent a delamination event, resulting in the detachment of only the primary cell wall. In this mechanism, crack propagation occurs on the inner side of the primary cell wall; however, it was also observed that it can extend into the outermost layers of the secondary cell wall as shown in Figure 3c. This figure illustrates the cross-section of a cell wall fragment, which is composed of multiple individual layers that could correspond to the secondary cell wall (S1) and primary cell wall. Furthermore, the presence of micro-cracks was observed on fragments of the cell wall (Figure 3c). Finally, cell rupture was identified as an additional failure mechanism, as shown in Figure 3d. As can be seen in the figure, this mechanism is characterized by the propagation of cracks through the cells, resulting in significant damage. The cell rupture can be attributed to two mechanisms: the impact of the mill blades on the particles and the collision of the particles with the mill walls. Consequently, this mechanism led to the observation of numerous fractured sclerenchyma cells (Figure 3e) and fragments of vascular bundles (Figure 3f) in the residue. The residue also contained numerous cell wall remnants, which are byproducts of the breakage of the primary and secondary cell walls. In Figure 3e, an isodiametric fractured cell can be clearly seen, displaying that this structural element is hollow (lumen) and possesses a thickened cell wall. Figure 3e also presents a magnified view of the cell wall, which displays a lamellar structure composed of layers of nanometer thickness (i.e., less than 200 nm). The ultrastructural characteristics described herein are consistent with the typical

characteristics of sclerenchyma cells and are responsible for their mechanical strength. In summary, different energy-absorbing mechanisms were identified, which are responsible for the structural and morphological characteristics of the hazelnut shell particles obtained by blade milling.

2.5. Distribution of the Biomolecules That Compose Hazelnut Shell Particles

CLSM images were obtained to examine the co-localization of cellulose/hemicellulose (blue regions) and lignin (green regions) in hazelnut shell particles (Figure 4). The microstructure observed in the CSLM images was consistent with the results of the SEM technique, where the following structures can be distinctly identified: tightly packed clusters of sclerenchyma cells (Figure 4a–d), whole single cells (Figure 4e,f), fractured single cells (Figure 4f), and cell wall and vascular bundles remnants (Figure 4f). Figure 4a–d showed that the cellulose/hemicellulose present in the form of microfibrils [27] is distributed uniformly throughout the cell wall, while lignin was mainly located in the compound middle lamella and in the outermost layers of the secondary cell wall (S1). These observations are consistent with those reported by several authors, who point out that in sclerenchyma tissues, lignin is mainly concentrated in the cell interface (i.e., junctions and edges cell) and that there is a gradient in lignin composition toward the interior of the cells [24,28,29]. Figure 4b clearly shows an intense fluorescence signal (green regions) associated with the high concentration of lignin located at the cell interface. Likewise, greater exposure of lignin was observed on the surfaces of particles composed of cell clusters (Figure 4c) and on whole single cells (Figure 4e). This phenomenon was also observed in the case of residue particles consisting of cell wall remnants and whole and fractured sclerenchyma cells (Figure 4f). On the other hand, the CLSM technique offers the distinct advantage of clearly and detailed displaying the ultrastructural and morphological characteristics of sclerenchyma cells. For instance, the cross-section of the cell wall can be clearly identified, which for this type of cell is characterized by being thickened. The cell wall thickness was 8.11 ± 2.17 µm. Other ultrastructural features that can be distinguished in CSLM images include pits and lumen, which are identified as areas devoid of fluorescence (Figure 4d). Furthermore, the distinction of sclerenchyma cell morphology was possible, with cells exhibiting an isodiametric and elongated shape, as shown in Figure 4c–e.

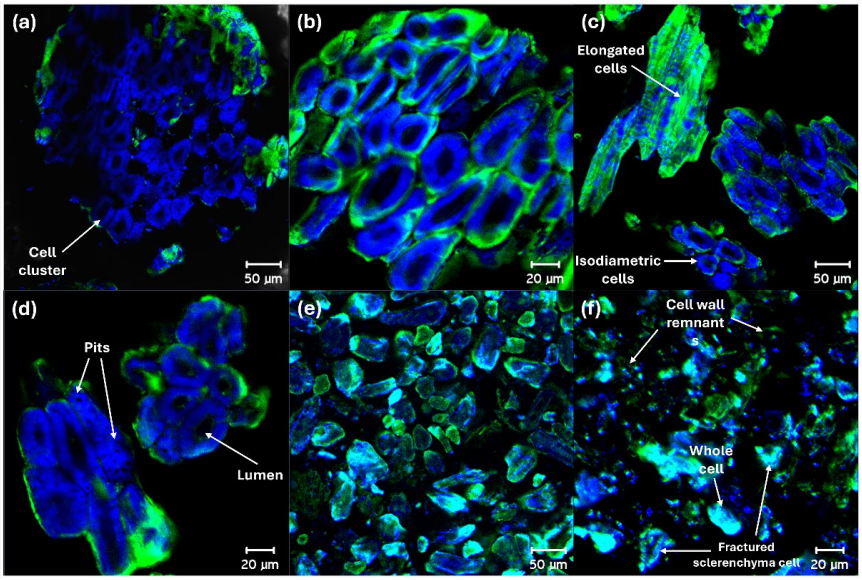

Figure 4. CSLM images showing the distribution of cellulose/hemicellulose (blue regions) and lignin (green regions) in hazelnut shell particles: (**a**) sieve$_{50}$, (**b**,**c**) sieve$_{100}$, (**d**) sieve$_{200}$, (**e**) sieve$_{400}$ and (**f**) residue.

Hazelnut shells are classified as lignocellulosic materials due to their high concentration of lignin, cellulose, and hemicellulose. According to the extant literature, the composition of hazelnut shells is as follows: lignin (30–38%), cellulose (17–24%), hemicellulose (15–28%), and moisture content (9%) [3]. The CLSM technique facilitates the examination of the spatial distribution of these biomolecules within the plant cells that constitute the shell. In summary, cellulose and hemicellulose are distributed uniformly throughout the cell wall, while lignin is primarily located in the middle lamella and the outermost regions of the secondary cell wall (S1). The increase in lignin exposure observed on the surface of sclerenchyma cells (either in clusters or individually) is a consequence of the breakage of the middle lamella, which caused minimal damage to the primary cell wall and allowed high amounts of lignin to remain on it. On the other hand, the mechanism involving the breakage of the primary and secondary cell walls is responsible for the generation of small fragments (cell wall remnants) rich in lignin, cellulose/hemicellulose, which correspond to residue particles. A comprehensive understanding of the co-localization of the biomolecules that comprise hazelnut shell particles is imperative for the optimal utilization of this type of agro-industrial waste, particularly in biorefinery processes aimed at the production of chemical compounds with high-added value. The fact that lignin is quite exposed on hazelnut shell particles could be advantageous in facilitating its extraction and subsequent reuse for the synthesis of polymers (e.g., epoxy resin and polyurethanes), carbon fibers, supercapacitor electrodes, and carbon foams [30]. In cases where hazelnut shell particles are utilized as fillers in the production of biocomposite materials, lignin exposure may emerge as a pivotal criterion for selecting a polymer matrix that is compatible with this biomolecule, thereby ensuring optimal interaction.

2.6. Evaluation of Roughness and Ultrastructure Cellular of the Hazelnut Shell Particles

Figure 5 shows a gallery of AFM topographic images of the surfaces of hazelnut shell particles retained in the used sieves. The topographical features observed on the surfaces of the particles are a consequence of the energy-absorbing mechanism that occur during the milling process. In this regard, the AFM images revealed that the surfaces of sclerenchyma cells, corresponding to the cell wall, exhibited a low degree of roughness (Figure 5a,b). As mentioned above, the middle lamella breakage does not result in substantial damage to the cell wall, which maintains its structural integrity. However, other samples exhibited rougher surfaces with stepped structures, which are associated with the breakage of the primary and secondary cell wall (Figure 5c,d). In cases where the damage to the cell wall is drastic and extends to the layers of the secondary cell wall, higher steps are generated. Furthermore, the multilayer structure of the cell wall could be discerned in fractured cells belonging to the residue, as shown in Figure 5f. Cell rupture is the mechanism responsible for generating fractured cells, which clearly exhibit the multilayered structure of the cell wall and its internal cavity, known as the lumen. The thickness of the layers was 267.44 $\pm$ 59.51 nm. This value is consistent with those reported by other authors for layers of sclerenchyma cells in walnut shell [28,29]. The size of the pits observed in the AFM images was 1.52 $\pm$ 0.37 µm (Figure 5b,d). This value is similar to the size of the pits found in sclerenchyma cells of walnut shells [29]. Furthermore, the particles in sieve$_{400}$ demonstrated significant roughness, which could be attributed to friction effects between the particles, as evidenced in Figure 5e.

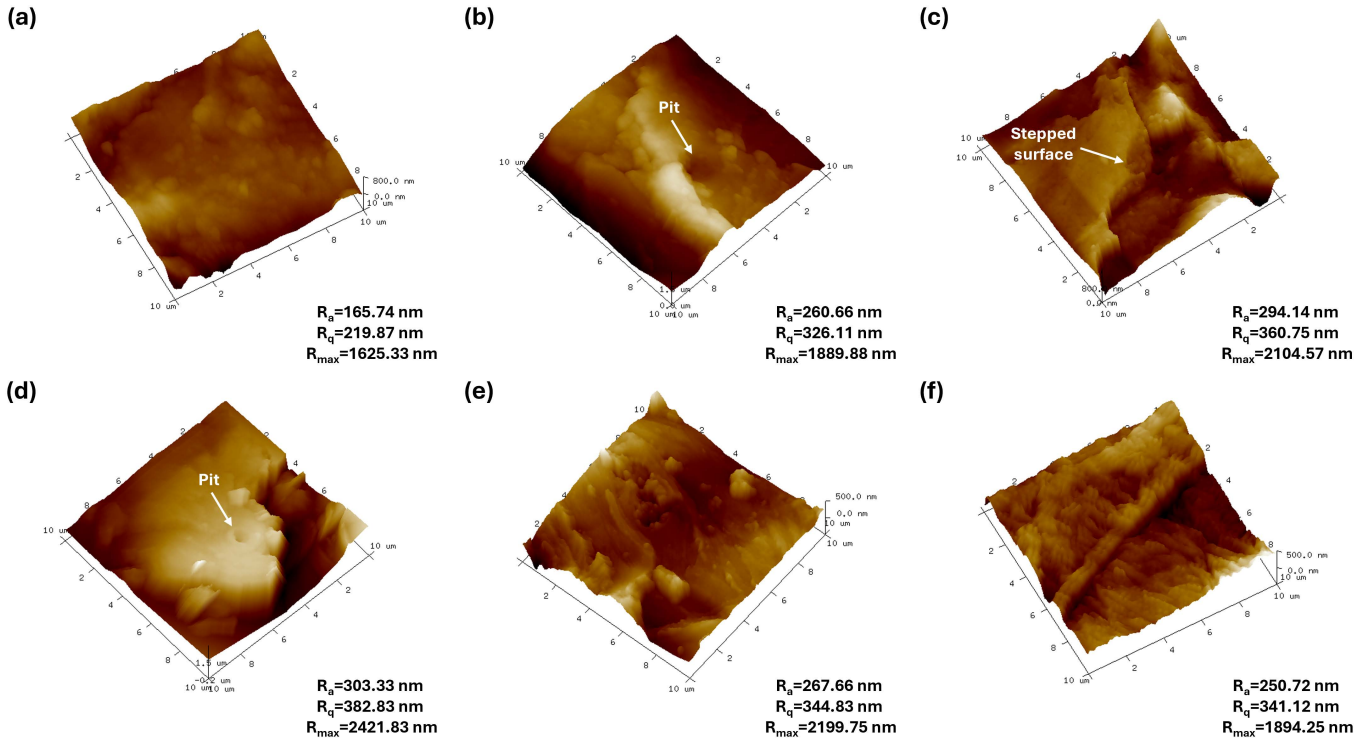

Figure 5. AFM topographic images (scanning area of 10 × 10 μm^2) and roughness parameters (R_a, R_q and R_{max}, n = 10) of the surfaces of hazelnut shell particles retained on each of the sieves used: (**a**) sieve$_{25}$, (**b**) sieve$_{50}$, (**c**) sieve$_{100}$, (**d**) sieve$_{200}$, (**e**) sieve$_{400}$ and (**f**) residue.

Roughness parameters were extracted from AFM images with a scan size of 10 × 10 μm^2 and are shown in Figure 5. The surfaces of sclerenchyma cells that retained their native structure and experienced minimal damage exhibited low roughness values (see Figure 5a). The values of R_a, R_q, and R_{max} were found to be 165.74 nm, 219.87 nm, and 1625.33 nm, respectively. In the AFM images displaying pits on the cell surfaces, an increase in the roughness parameter values was observed (Figure 5b). AFM images demonstrating damaged cell wall surfaces (Figure 5e) or the cross-section of this organelle (Figure 5f) also exhibited elevated roughness values in comparison to intact surfaces. Lastly, AFM analyses revealed that surfaces with stepped structures associated with cell wall breakage exhibited elevated levels of surface roughness, as shown in Figure 5c,d. For instance, R_{max} values greater than 2000 nm were observed on surfaces with stepped structures. To our knowledge, studies focused on topographic analyses of hazelnut shell particle surfaces are limited. Balasundar et al. [31] reported R_a, R_q, and R_{max} values of 27.94 nm, 35.16 nm, and 180.34 nm, respectively, for pistachio shell particles. These values are considerably lower than those found for hazelnut shell particles. Consequently, this study presents novel findings concerning topographical characteristics and roughness parameters of hazelnut shell particles, which are associated with failure mechanisms. Roughness is a surface characteristic that could be very relevant for some applications of agro-industrial waste particles. In recent years, particles derived from agro-industrial waste have gained significant importance due to their potential application as abrasive particles in the production of exfoliating cosmetic products. The abrasive capacity of these particles depends on their size, morphology, and surface roughness. It is hypothesized that, based on the roughness parameters obtained, stepped surfaces would have greater abrasion capacity compared to smoother surfaces.

3. Materials and Methods

3.1. Plant Material and Milling Experiments

Whole hazelnuts (*Corylus avellana* L.) imported from the USA, were purchased at a local market in Mexico City (Mexico). The hazelnut shell was separated from the kernel using a bench vise. The shells were washed with tap water to remove dirt and impurities. The shells were then oven-dried at 40 °C for 12 h. An electric blade grinder (CG-300, Cgoldenwall, Hong Kong, China) with a rotation speed of 28,000 rpm was used for the milling experiments. Blade mills are characterized by their simplicity and cost-effectiveness, and they require minimal maintenance. The maximum capacity of the used miller is 300 g. The milling times tested were 0.5, 1 and 1.5 min; the times were continuous and there were no rest periods. The experiments were conducted under dry conditions, and the temperature in the milling chamber never exceeded 50 °C. Approximately 50 g of hazelnut shells were used to carry out the milling experiments. For each milling condition, a total of five replicates were made. Milled shell samples were stored in hermetically sealed polyethylene bags for further analysis.

3.2. Particle Size Distribution by Sieving Methodology

The particle size distribution (PSD) of the milled hazelnut shell samples was determined by means of sieving methodology. Approximately 50 g of milled material were utilized in the analyses, which were segregated on a set of five standard stainless-steel sieves (8-inche diameter): 25, 50, 100, 200, and 400 (ASTM E11, WS Tyler, Mentor, OH, USA). The characteristics and nominal opening of each sieve utilized are shown in Table 4. The minimum diameter (D_{min}) of the class corresponds to the nominal opening value of the sieve utilized, and the particles retained in that class will exceed that value. On the contrary, the maximum diameter (D_{max}) is defined as the nominal opening value of the previous sieve, and the particles will be smaller than or equal to this value. The average class size (D_i) is defined by Equation (1).

$$D_i = \frac{D_{max} + D_{min}}{2} \quad (1)$$

Table 4. Classes and characteristics of the sieves used for the evaluation of particle size distribution (PSD).

No. of Classes	Standard Sieve No.	Nomenclature Used in This Study	Minimum Diameter D_{min} (μm) (Sieve Opening)	Maximum Diameter, D_{max} (μm)	Average Class Size D_i (μm)
1	25	$Sieve_{25}$	710	1700 *	1205
2	50	$Sieve_{50}$	300	710	505
3	100	$Sieve_{100}$	150	300	225
4	200	$Sieve_{200}$	75	150	112.5
5	400	$Sieve_{400}$	38	75	56.5
6	Residue	Residue	20 *	≤38	29

* The maximum diameter of the $sieve_{25}$ and the minimum diameter of the residue were determined by referencing the opening values of sieve No. 12 (1.7 mm) and No. 635 (20 μm), respectively.

These sieves were then sorted according to sieve opening and subsequently shaken for ten minutes. The fraction of mass retained in each sieve was calculated using Equation (2), and these values were used to plot the histograms of PSD.

$$Mass\ fraction\ (\%) = \frac{Mass\ retained\ on\ sieve}{Total\ sample\ mass} \times 100 \quad (2)$$

Furthermore, the mean particle size (D_{mean}) and standard deviation (σ) were estimated for each milling condition using Equations (3) and (4), respectively. A mathematical way to quantify the spread of a distribution is by calculating the standard deviation (σ).

$$D_{mean} = \frac{\sum n_i D_i}{\sum n_i} \tag{3}$$

$$\sigma = \left(\frac{\sum n_i (D_i - D_{mean})^2}{\sum n_i} \right)^{1/2} \tag{4}$$

According to the aforementioned equations, n_i and D_i correspond to the retained mass fraction (%) and average class size (µm), respectively. Consequently, cumulative mass fraction curves were plotted to calculate the D_{10}, D_{50}, and D_{90} percentiles (µm). The median size at the 50% percentile (D_{50}) is the size that marks the midpoint of the cumulative distribution curve. Conversely, the particle sizes at the 10% percentile (D_{10}) and 90% percentile (D_{90}) are employed to denote the size of the smallest and largest particles, respectively. The *span* parameter was calculated using Equation (5), which is an indicator for quantifying the spread of the distribution.

$$Span = \frac{D_{90} - D_{10}}{D_{50}} \tag{5}$$

The parameters D_{mean}, σ, and *span* were calculated to quantitatively characterize the granulometry of the milled shell samples at different times. The powders retained in each of the sieves derived from the separation process were collected and stored in hermetically sealed polyethylene bags. Each of these fractions was evaluated for their flowability parameters, and the morphology and microstructure of the particles were examined using different microscopy techniques.

3.3. Determination of Flowability Parameters

The flowability of each of the fractions retained in the sieves were determined by measuring some parameters, including the Carr index (*CI*), Hausner ratio (*HR*), and angle of repose (*AOR*). To calculate the *CI* and *HR* values, the apparent (ρ_A) and tapped (ρ_T) densities of each powder are first determined. To calculate both densities, the method described by Düsenberg et al. [21] was followed with some modifications. To determine the ρ_A, a graduated measuring cylinder of 25 cm^3 was filled with powder until a volume of 10 cm^3 was reached, and the weight was recorded. Subsequently, the cylinder was manually tapped 100 times on a flat surface and the new volume was recorded to calculate the ρ_T. Both densities were calculated using the ratio of the weight of the powder to its respective volume. The *CI* and *HR* parameters were calculated using Equations (6) and (7), respectively.

$$CI\ (\%) = \frac{\rho_T - \rho_A}{\rho_T} \times 100 \tag{6}$$

$$HR = \frac{\rho_T}{\rho_A} \tag{7}$$

On the other hand, the *AOR* was determined using the funnel method. A symmetrical plastic funnel with an angle of 55° and an internal diameter of 6 mm was placed at a fixed separation distance of 7 cm above the flat surface. 20 g of each sample were carefully poured onto the funnel, and the height (h) and diameter (D) of the cone formed were measured to calculate the AOR using Equation (8). The flowability parameters (*CI*, *HR* and *AOR*) were determined in quintupled for all powders retained on the sieves.

$$tan\ \alpha = \frac{2h}{D} \tag{8}$$

3.4. Evaluation of Size and Shape Parameters by Image Analysis

An evaluation of the size and morphology of the fractions retained in the sieves was conducted using optical microscopy and image analysis. Firstly, the particles were meticulously placed and dispersed on a clean microscope slide. Subsequent digital images of the particles, observed at 5× magnification, were captured using a light microscope (BX51, Olympus, Tokyo, Japan) equipped with a digital camera (Infinity, Lumenera, Ottawa, ON, Canada). A total of 10 images for each of the fractions were obtained under the same lighting settings. The RGB images were stored in BMP format with a resolution of 1280 × 1024 pixels. Image analysis was performed using the ImageJ software (v. 1.45s, National Institutes Health, Bethesda, MD, USA, ImageJ). First, the scale of the images was changed from pixels to micrometers using a reference pattern. Then, the RGB images (32-bit) were converted to grayscale images (8-bit) using the "Type 8-bit" tool. To segment the particles, which constituted the region of interest within the image, the "Threshold" tool was employed, setting a grayscale value for pixels from 0 to 90. Finally, several parameters relating to size (area, perimeter, Feret's diameter) and shape (circularity, aspect ratio, roundness) particles were measured using the "Analyze Particles" tool.

3.5. Scanning Electron Microscopy (SEM)

The morphology and microstructure of the particles were examined using a scanning electron microscope (JSM-7800F, JEOL, Tokyo, Japan). The particles were deposited onto sample holder using conductive double-sided carbon tape, and then a thin layer of carbon was applied to the particles. The images of the particles were obtained at varying magnifications using a secondary electron detector with an acceleration voltage of 5 kV and a working distance of approximately 10 mm. A set of measurements were collected to determine the dimensions of the various types of sclerenchyma cells that comprise the particles.

3.6. Confocal Laser Scanning Microscopy (CLSM)

The co-localization of lignin and cellulose/hemicellulose in hazelnut shell particles was examined using a CLSM (LSM 710 NLO, Carl Zeiss, Oberkochen, Germany). The samples were stained using the methodologies proposed by Bond et al. [32] and Nicolás-Bermúdez et al. [29]. For the detection of cellulose/hemicellulose, the particles were stained with a 1% aqueous solution (v/v) of white calcofluor M2R (fluorescent brightener 28 F3543, Sigma-Aldrich, St. Louis, MO, USA). On the other hand, lignin detection required staining with a 1% aqueous solution (w/v) of safranin (safranine O U926-03, J. T. Baker, Phillipsburg, NJ, USA). The samples were stained for 10 min and then the excess fluorochrome was removed with distilled water. The samples were dried at room temperature for 24 h. Spectral channel mode was used for simultaneous detection of biomolecule fluorescence, using excitation wavelengths for calcofluor (blue) and safranin (green) of 405 nm and 488 nm, respectively. The samples were observed using an objective lens (Plan-Neofluar 10 × /0.3, Carl Zeiss, Oberkochen, Germany) with different values of optical zoom and the resolution of the captured images was 1024 × 1024 pixels (TIFF format).

3.7. Atomic Force Microscopy (AFM)

The surface and roughness of the particles were examined using an atomic force microscope (Multimode V connected to a Nanoscope V microcontroller, Bruker, Santa Barbara, CA, USA). The particles retained in the different sieves were meticulously deposited onto a magnetic holder using double-sided adhesive tape. The samples were analyzed in tapping mode using RTESP-300 probes (Bruker, Camarillo, CA, USA). Topographic images of different scanning areas were captured on various particles corresponding to

each of the fractions obtained. The processing of the AFM images and the estimation of the roughness parameters (R_a, R_q and R_{max}) were performed using the NanoScope Analysis v 1.4 software (Bruker, Santa Barbara, CA, USA). The roughness parameters were extracted from the topographic images with the largest scanning area (10 × 10 μm^2).

3.8. Statistical Analysis

The values of all parameters obtained were expressed as means ± standard deviations. Tukey tests were performed using the statistical software SigmaPlot v. 15.0 (Graffiti LLC, Palo Alto, CA, USA) to establish statistical differences ($p < 0.05$) between the different parameters measured.

4. Conclusions

This study presents novel findings on the milling process of hazelnut (*Corylus avellana* L.) shell waste and the physicochemical characteristics of the resulting particles. The results demonstrated that, under the specific milling conditions that were examined, the initial dimensions of the shells were effectively reduced. The shells milled for 1.5 min had a D_{mean} of 281.58 μm with a σ of 316.78 μm; the high σ value was associated with the wide dispersion of particle sizes that were generated (≤1.7 mm). The flowability results indicated that the particles retained from sieve$_{100}$ to residue exhibited a poor or null flow character. Regarding morphological analysis, it was observed that the particles have complex shapes and that there was an increase in aspect ratio values when the particle size was finer. The microstructures of the hazelnut shell particles were identified using SEM and CLSM techniques: tightly packed clusters of sclerenchyma cells (sieve$_{25}$ to sieve$_{200}$), large single cells and clusters of small cells (sieve$_{400}$), whole and fractured isodiametric cells, and fragments of cell walls and vascular bundles (residue). A comprehensive analysis was conducted using microscopic techniques to identify several energy-absorbing mechanisms occurring during the milling process. The results revealed that the middle lamella breakage was the predominant mechanism responsible for the fragmentation of the hazelnut shell. The failure mechanisms identified in the images are responsible for the morphological and microstructural characteristics, roughness parameters, and increased exposure of lignin on the cell surface. The knowledge generated in this study could be used as selection criteria for the optimal application of hazelnut shell particles, thereby reducing their environmental impact and increasing their revalorization.

Author Contributions: Conceptualization, I.A.-V. and J.V.M.-M.; methodology, R.N.D.-F., M.B.G.-P. and D.A.-B.; software, I.A.-V. and J.V.M.-M.; validation, J.J.C.-P. and N.V.-R.; formal analysis, I.A.-V., J.V.M.-M. and G.A.R.-C.; investigation, I.A.-V.; resources, I.A.-V. and J.V.M.-M.; data curation, G.A.R.-C.; writing—original draft preparation, I.A.-V., J.V.M.-M., R.N.D.-F. and G.A.R.-C.; writing—review and editing, I.A.-V., J.V.M.-M., M.B.G.-P., D.A.-B. and J.J.C.-P.; visualization, I.A.-V. and J.V.M.-M.; supervision, I.A.-V.; project administration, I.A.-V.; funding acquisition, I.A.-V. and J.V.M.-M. All authors have read and agreed to the published version of the manuscript.

Funding: This research was funded by the Instituto Politécnico Nacional (IPN-México), grant numbers: 20240509, 20251050, 20251166.

Data Availability Statement: The original contributions presented in this study are included in the article. Further information can be obtained from the corresponding author.

Acknowledgments: We would also like to thank the Centro de Nanociencias y Micro y Nanotecnologías (CNMN-IPN) for allowing us to use their laboratories to conduct this study. Additionally, we would like to express our gratitude to Natalia Gutiérrez-Aldana for her invaluable support.

Conflicts of Interest: The authors declare no conflicts of interest.

Abbreviations

The following abbreviations are used in this manuscript:

PSD	Particle size distribution
SEM	Scanning electron microscopy
AFM	Atomic force microscopy
CLSM	Confocal laser scanning microscopy
CI	Carr index
HR	Hausner ratio
AOR	Angle of repose

References

1. Barczewski, M.; Sałasińska, K.; Szulc, J. Application of Sunflower Husk, Hazelnut Shell and Walnut Shell as Waste Agricultural Fillers for Epoxy-Based Composites: A Study into Mechanical Behavior Related to Structural and Rheological Properties. *Polym. Test.* **2019**, *75*, 1–11. [CrossRef]
2. Jan, K.; Riar, C.S.; Saxena, D.C. Characterization of Agro-Industrial Byproducts and Wastes for Sustainable Industrial Application. *J. Food Meas. Charact.* **2017**, *11*, 1254–1265. [CrossRef]
3. McNeill, D.C.; Pal, A.K.; Nath, D.; Rodriguez-Uribe, A.; Mohanty, A.K.; Pilla, S.; Gregori, S.; Dick, P.; Misra, M. Upcycling of Ligno-Cellulosic Nutshells Waste Biomass in Biodegradable Plastic-Based Biocomposites Uses—A Comprehensive Review. *Compos. Part C Open Access* **2024**, *14*, 100478. [CrossRef]
4. Aguado-González, L.; Sierra-Pérez, J.; Forte, C.; López-Forniés, I.; Blanc, S. Cascade Valorization of Hazelnut Industry By-Products for Industrial Use through Co-Creative Processes. *J. Clean. Prod.* **2025**, *494*, 144989. [CrossRef]
5. Allegrini, A.; Salvaneschi, P.; Schirone, B.; Cianfaglione, K.; Michele, A.D. Multipurpose Plant Species and Circular Economy: *Corylus avellana* L. as a Study Case. *Front. Biosci. Landmark* **2022**, *27*, 11. [CrossRef]
6. Huss, J.C.; Antreich, S.J.; Bachmayr, J.; Xiao, N.; Eder, M.; Konnerth, J.; Gierlinger, N. Topological Interlocking and Geometric Stiffening as Complementary Strategies for Strong Plant Shells. *Adv. Mater.* **2020**, *32*, 2004519. [CrossRef]
7. Agilee, N.; Spasojević, T.; Delić, M.; Ogrizović, Đ.; Gria, I.R.; Prlainović, N.; Đolić, M. Hazelnut Shells as a Tenable Biosorbent for Basic Red 18 Azo Dye Removal. *Separations* **2024**, *11*, 343. [CrossRef]
8. Balci, S.; Doğu, T.; Yücel, H. Characterization of Activated Carbon Produced from Almond Shell and Hazelnut Shell. *J. Chem. Technol. Biotechnol.* **1994**, *60*, 419–426. [CrossRef]
9. Şencan, A.; Karaboyacı, M.; Kılıç, M. Determination of Lead(II) Sorption Capacity of Hazelnut Shell and Activated Carbon Obtained from Hazelnut Shell Activated with $ZnCl_2$. *Environ. Sci. Pollut. Res.* **2015**, *22*, 3238–3248. [CrossRef]
10. Ebrahimi, R.; Fathi, M.; Ghoddusi, H.B. Pickering Emulsions Stabilized by Cellulose Nanocrystals Extracted from Hazelnut Shells: Production and Stability under Different Harsh Conditions. *Int. J. Biol. Macromol.* **2024**, *258*, 128982. [CrossRef]
11. Aliotta, L.; Vannozzi, A.; Bonacchi, D.; Coltelli, M.-B.; Lazzeri, A. Analysis, Development, and Scaling-Up of Poly(Lactic Acid) (PLA) Biocomposites with Hazelnuts Shell Powder (HSP). *Polymers* **2021**, *13*, 4080. [CrossRef]
12. Hebda, T.; Brzychczyk, B.; Francik, S.; Pedryc, N. Evaluation of Suitability of Hazelnut Shell Energy for Production of Biofuels. *Eng. Rural Dev.* **2018**, *17*, 1860–1865.
13. Tareq Noaman, A.; Abed, M.S.; Al-Gebory, L.; Al-Zubaidi, A.B.; Al-Tabbakh, A.A. Production of Agro-Waste Cement Composites: Influence of Nutshells on Mechanical and Hardened Properties. *Constr. Build. Mater.* **2023**, *394*, 132137. [CrossRef]
14. Martínez, B.G. *Materiales Avanzados y Nanomateriales: Aprovechamiento de Fuentes Naturales y Sus Beneficios al Medio Ambiente*, 1st ed.; Universidad Autónoma del Estado de México, Vigueras Santiago, E., Eds.; OmniaScience: Barcelona, Spain, 2022; ISBN 978-84-123480-3-3.
15. Sitotaw, Y.W.; Habtu, N.G.; Gebreyohannes, A.Y.; Nunes, S.P.; Van Gerven, T. Ball Milling as an Important Pretreatment Technique in Lignocellulose Biorefineries: A Review. *Biomass Convers. Biorefinery* **2023**, *13*, 15593–15616. [CrossRef]
16. Gorrasi, G.; Sorrentino, A. Mechanical Milling as a Technology to Produce Structural and Functional Bio-Nanocomposites. *Green Chem.* **2015**, *17*, 2610–2625. [CrossRef]
17. Haykiri-Acma, H.; Baykan, A.; Yaman, S.; Kucukbayrak, S. Effects of Fragmentation and Particle Size on the Fuel Properties of Hazelnut Shells. *Fuel* **2013**, *112*, 326–330. [CrossRef]
18. Hemmati, N.; Sheikhmozafari, M.J.; Taban, E.; Tajik, L.; Faridan, M. Pistachio Shell Waste as a Sustainable Sound Absorber: An Experimental and Empirical Investigation. *Int. J. Environ. Sci. Technol.* **2024**, *21*, 4867–4880. [CrossRef]

19. Tahmaz, J.; Begić, M.; Oručević Žuljević, S.; Mehmedović, V.; Alkić-Subašić, M.; Jurković, J.; Djulančić, N. Physical Properties of Vegetable Food Seasoning Powders. In *10th Central European Congress on Food*; Brka, M., Sarić, Z., Oručević Žuljević, S., Omanović-Mikličanin, E., Taljić, I., Biber, L., Mujčinović, A., Eds.; Springer International Publishing: Cham, Switzerland, 2022; pp. 14–32.
20. Traina, K.; Cloots, R.; Bontempi, S.; Lumay, G.; Vandewalle, N.; Boschini, F. Flow Abilities of Powders and Granular Materials Evidenced from Dynamical Tap Density Measurement. *Powder Technol.* **2013**, *235*, 842–852. [CrossRef]
21. Düsenberg, B.; Schmidt, J.; Sensoy, I.; Bück, A. Flowability of Plant Based Food Powders: Almond, Chestnut, Chickpea, Coconut, Hazelnut and Rice. *J. Food Eng.* **2023**, *357*, 111606. [CrossRef]
22. Shah, D.S.; Moravkar, K.K.; Jha, D.K.; Lonkar, V.; Amin, P.D.; Chalikwar, S.S. A Concise Summary of Powder Processing Methodologies for Flow Enhancement. *Heliyon* **2023**, *9*, e16498. [CrossRef]
23. Kaleem, M.A.; Alam, M.Z.; Khan, M.; Jaffery, S.H.I.; Rashid, B. An Experimental Investigation on Accuracy of Hausner Ratio and Carr Index of Powders in Additive Manufacturing Processes. *Met. Powder Rep.* **2021**, *76*, S50–S54. [CrossRef]
24. Tao, S.; Khanizadeh, S.; Zhang, H.; Zhang, S. Anatomy, Ultrastructure and Lignin Distribution of Stone Cells in Two *Pyrus* Species. *Plant Sci.* **2009**, *176*, 413–419. [CrossRef]
25. Zamil, M.S.; Geitmann, A. The Middle Lamella—More than a Glue. *Phys. Biol.* **2017**, *14*, 015004. [CrossRef]
26. Flores-Johnson, E.A.; Carrillo, J.G.; Zhai, C.; Gamboa, R.A.; Gan, Y.; Shen, L. Microstructure and Mechanical Properties of Hard Acrocomia Mexicana Fruit Shell. *Sci. Rep.* **2018**, *8*, 9668. [CrossRef]
27. Bogolitsyn, K.G.; Zubov, I.N.; Gusakova, M.A.; Chukhchin, D.G.; Krasikova, A.A. Juniper Wood Structure under the Microscope. *Planta* **2015**, *241*, 1231–1239. [CrossRef]
28. Xiao, N.; Felhofer, M.; Antreich, S.J.; Huss, J.C.; Mayer, K.; Singh, A.; Bock, P.; Gierlinger, N. Twist and Lock: Nutshell Structures for High Strength and Energy Absorption. *R. Soc. Open Sci.* **2021**, *8*, 210399. [CrossRef]
29. Nicolás-Bermúdez, J.; Arzate-Vázquez, I.; Chanona-Pérez, J.J.; Méndez-Méndez, J.V.; Perea-Flores, M.J.; Rodríguez-Castro, G.A.; Domínguez-Fernández, R.N. Characterization of the Hierarchical Architecture and Micromechanical Properties of Walnut Shell (*Juglans regia* L.). *J. Mech. Behav. Biomed. Mater.* **2022**, *130*, 105190. [CrossRef]
30. Wang, X.; Leng, W.; Nayanathara, R.M.O.; Milsted, D.; Eberhardt, T.L.; Zhang, Z.; Zhang, X. Recent Advances in Transforming Agricultural Biorefinery Lignins into Value-Added Products. *J. Agric. Food Res.* **2023**, *12*, 100545. [CrossRef]
31. Balasundar, P.; Narayanasamy, P.; Senthil, S.; Abdullah Al-Dhabi, N.; Prithivirajan, R.; Shyam Kumar, R.; Ramkumar, T.; Subrahmanya Bhat, K. Physico-Chemical Study of Pistachio (Pistacia Vera) Nutshell Particles as a Bio-Filler for Eco-Friendly Composites. *Mater. Res. Express* **2019**, *6*, 105339. [CrossRef]
32. Bond, J.; Donaldson, L.; Hill, S.; Hitchcock, K. Safranine Fluorescent Staining of Wood Cell Walls. *Biotech. Histochem.* **2008**, *83*, 161–171. [CrossRef]